STATE OF THE CLIMATE IN 2010

J. Blunden, D. S. Arndt, and M. O. Baringer, Eds.

Associate Eds. K. M. Willett, A. J. Dolman, B. D. Hall, P. W. Thorne, J. M. Levy, H. J. Diamond, J. Richter-Menge, M. Jeffries, R. L. Fogt, L. A. Vincent, and J. M. Renwick

Special Supplement to the
Bulletin of the American Meteorological Society
Vol. 92, No. 6, June 2011

6. ANTARCTICA

a. Overview—R. L. Fogt

The calendar year 2010 contained many record Antarctic climate anomalies. In particular, the austral winter was characterized by low pressure anomalies across the high southern latitudes and enhanced circumpolar zonal flow. This spatial pattern is consistent with a strong positive Southern Hemisphere Annular Mode (SAM) index. Although this pattern weakened in September, it strengthened again in October and remained positive throughout the rest of the year. A La Niña began in the tropical Pacific in July, which further amplified the low pressure anomalies particularly in the South Pacific/West Antarctic sector. The strength (in a statistical sense) and persistence of low pressure anomalies across much of Antarctica during austral winter and in the last part of 2010 gave rise to many record anomalies in sea ice extent, surface pressure, and temperature, while keeping continent-wide snow melt and precipitation values below climatological averages. Specific highlights in 2010 include:

- A record positive austral winter (June–August) averaged SAM index, and a record positive November SAM index. These records are based on the Marshall (2003) index, which now spans over 50 continuous years.
- Records of minimum pressure observed at many stations across Antarctica during the austral winter, and on the Antarctic Peninsula, above-average temperatures from May–December and record strong winds during June and October–November. In the northern Antarctic Peninsula, the below-average temperatures that began in April 2009 ended in March 2010 with the start of an above-average temperature period lasting throughout the rest of the year.
- Lower precipitation across Antarctica in general compared to 2009. The conditions were most different in coastal West Antarctica and the southern Antarctic Peninsula, where the simultaneous occurrence of La Niña-influenced conditions and enhanced cyclonic activity drastically altered the regional circulation.
- Surface snow melt in austral summer 2009/10 rebounded somewhat from its record low in austral summer 2008/09, but still remained well below the 30-year average based on satellite passive microwave records.
- Record high values of zonally-averaged sea ice extent from mid-June through late August and again from mid-November through early December. These records are based on over 30 years of data from satellite measurements of sea ice extent.
- A smaller than average, but unusually persistent, Antarctic ozone hole. The maximum area of the Antarctic hole peaked on 25 September 2010, but low ozone values persisted until mid-December 2010.

b. Circulation—A. J. Wovrosh, S. Barreira, and R. L. Fogt

The Antarctic large-scale circulation during 2010, based on NCEP/NCAR reanalysis data, is examined using a vertical cross-section of polar-cap averaged (60°S–90°S) geopotential height and temperature, and circumpolar (50°S–70°S) zonal wind anomalies within the troposphere and stratosphere (Fig. 6.1), as well as surface pressure and surface temperature anomalies (Fig. 6.2). Since the start of the modern satellite era, reanalysis data quality has improved drastically in southern high latitudes especially for circulation related fields (Bromwich and Fogt 2004; Bromwich et al. 2007), thus reanalysis data beginning in 1979 is used here. As in previous reports, the year was divided into periods where the circulation anomalies were fairly consistent (January–April, May–August, September–November, and December).

From Fig. 6.1, January–March were marked with above-average height/pressure anomalies over Antarctica, which were > 1 standard deviation from the 1979–2008 mean up to 30 hPa. At the surface, above-average pressures were observed across much of the continent but not the Peninsula (Fig. 6.2a). In terms of surface temperature, the Antarctic continent was warmer than average in the first part of the year (many places > 2 standard deviations from the 1979–2008 mean), while the northern Antarctic Peninsula was below average (Fig. 6.2b). In particular, the high temperature anomalies at South Pole in early 2010 make the previous long-term cooling trend there statistically insignificant. These circulation anomaly patterns are consistent with an El Niño influence on the Antarctic climate (i.e., Turner 2004), which lasted through the first part of 2010, and a negative Southern Hemisphere Annular Mode (SAM) index, which was the lowest in February (Fig. 6.1c, based on the Marshall (2003) index). The 2009–10 El Niño marked the highest sea surface temperature anomalies in the central equatorial Pacific in the last three decades (Lee and McPhaden 2010), and this event has been linked

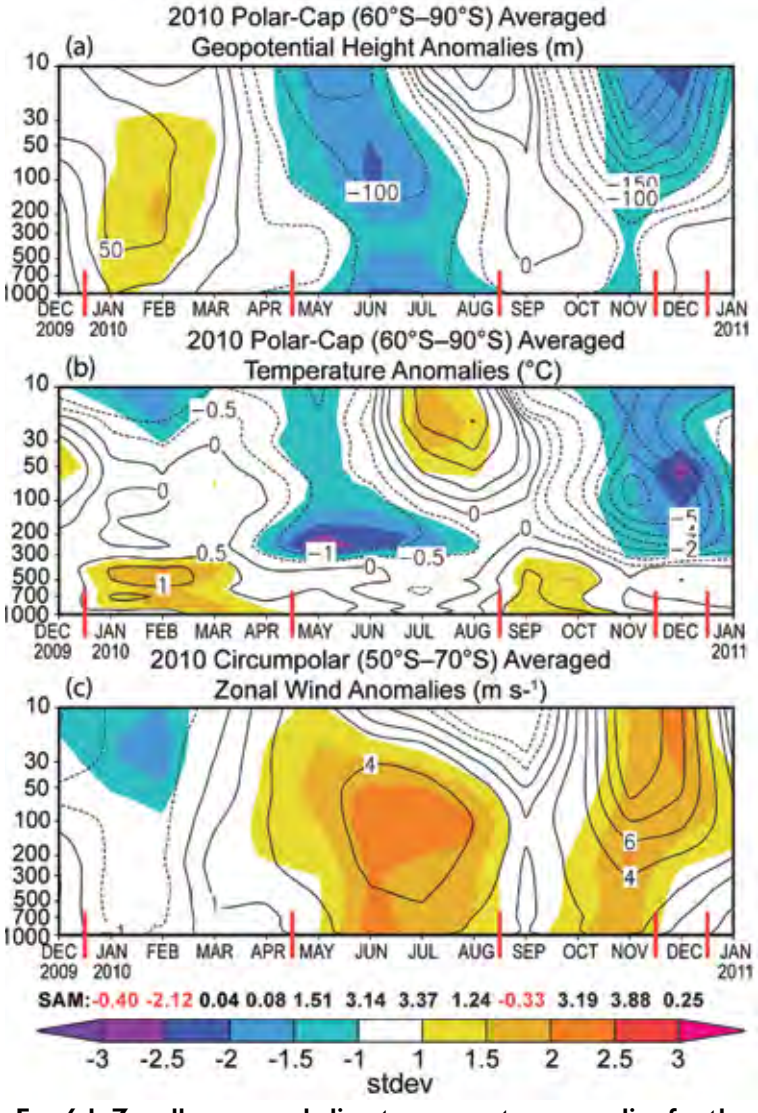

Fig. 6.1. Zonally-averaged climate parameter anomalies for the southern polar region in 2010 relative to the 1979–2008 period: (a) polar cap (60°S–90°S) averaged geopotential height anomalies (m); (b) polar cap averaged temperature anomalies (°C); (c) circumpolar (50°S–70°S) averaged zonal wind anomalies (m s^{-1}). The shading represents how many standard deviations the anomalies are from the 1979–2008 mean (color bar at bottom for scale). Red vertical bars indicate the four separate climate periods shown as spatial climate anomalies in Fig. 6.2. Primary contour interval is 50 m in (a), 1°C in (b), and 2 m s^{-1} in (c), with additional contours at ± 25 m, ± 0.5°C, and ± 1 m s^{-1} in (a), (b), and (c), respectively. Values for the SAM index are shown along the bottom in black and red. (Source: NCEP/NCAR reanalysis.)

to the high temperature anomalies in West Antarctica in 2010 (Fig. 6.2a; Lee et al. 2010). More generally, the warming in the central tropical Pacific has recently been linked to the overall warming trend in West Antarctica (Ding et al. 2011; Schneider et al. 2011).

A shift in the circulation pattern occurred in the austral winter, as negative geopotential height anomalies extended from the surface to 10 hPa over the polar cap (Fig. 6.1a). At the surface, this pattern of lower than average pressures is observed across nearly all of the high southern latitudes south of 60°S (especially off the coast of West Antarctica), while above-average pressure anomalies are observed throughout much of the southern midlatitudes (Fig. 6.2c). Such pressure decreases over Antarctica and increases in the midlatitudes strengthen the meridional pressure gradient, and therefore the circumpolar zonal flow was much stronger than average (> 2 standard deviations from the 1979–2008 mean) throughout the troposphere and into the lower stratosphere during austral winter in 2010 (Fig. 6.1c). These austral winter circulation anomalies are consistent with a strong positive SAM index (Fig. 6.1c). Indeed, the austral winter SAM index (an average value of 2.58 for June–August) was the highest value based on the 50+ year record of Marshall (2003). The temperature patterns in winter were less straightforward; there were negative polar-cap averaged temperature anomalies at 300 hPa < 2 standard deviations below the 1979–2008 mean throughout much of the winter, with higher-than-average temperatures above 100 hPa in late winter (July–August; Fig. 6.1b). Meanwhile, above-average temperatures were observed within the Weddell Sea region (Fig. 6.2d), which aided in generating negative winter sea ice anomalies in the northern Weddell Sea and Bellingshausen Seas (section 6f).

The low pressure and geopotential height anomalies across Antarctica weakened considerably in September (Fig. 6.1a), in turn weakening the meridional pressure gradient and thus the circumpolar zonal wind (Fig. 6.1c). From October to November, the pattern observed during the winter re-emerged, as polar-cap averaged geopotential heights were again negative, circumpolar zonal winds were again above average, and the Marshall (2003) SAM index reached another record in November. Of particular note are the spring surface temperature anomalies (Fig. 6.2f). The enhancement of above-average surface pressure in the midlatitudes east of

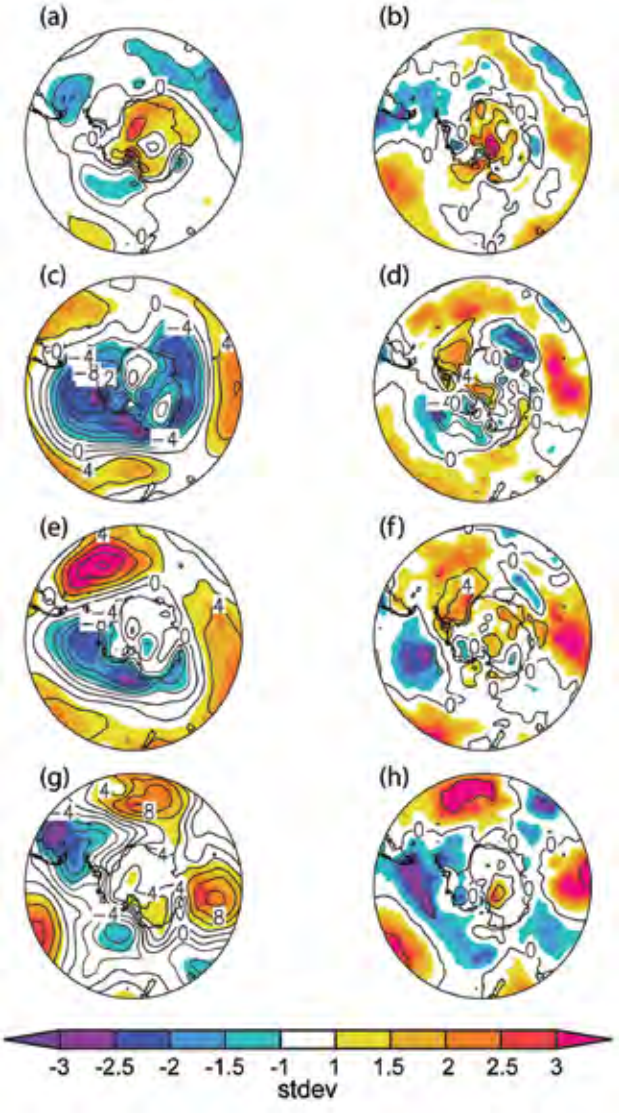

Fig. 6.2. (Left) Surface pressure anomaly and (right) surface temperature anomaly contours (in hPa and °C, respectively) relative to 1979–2008 climatology for (a,b) January–April 2010; (c,d) May–August 2010; (e,f) September–November 2010; (g,h) December 2010. The shaded regions correspond to the number of standard deviations the anomalies are from the 1979–2008 mean, as in Fig. 6.1. (Source: NCEP/NCAR reanalysis.)

South America (> 3.0 standard deviations) coupled with the low pressure west of the Antarctic Peninsula (Fig. 6.2e) generated northerly flow anomalies onto the Peninsula and Weddell Sea region, leading to the marked warming there in the austral spring (Fig. 6.2f; also reflected in polar-cap temperatures up to 500 hPa in Fig. 6.1b). The pattern of pressure anomalies in the Pacific and Atlantic sectors of Fig. 6.2e resemble a wave-train of pressure anomalies across the Pacific sector, a feature commonly observed during strong La Niña events (Turner 2004).

December was separated from the other months due to its unique circulation anomalies. Figure 6.1 shows below-average polar-cap temperatures and geopotential heights above 300 hPa and 50 hPa, respectively, and stronger-than-average circumpolar zonal winds > 1.5 standard deviations from the 1979–2008 mean above 300 hPa. At the surface, the wave-train of pressure anomalies is still observed (Fig. 6.2g), but its location in comparison to Fig. 6.2e acts to generate more southerly (cold) flow extending from the South Pacific across the Antarctic Peninsula, driving the very strong below average temperature anomalies there in December (Fig. 6.2h).

c. Surface Manned and Automatic Weather Station Observations—S. Colwell, L. M. Keller, and M. A. Lazzara

In general, both the automatic and manned stations (see Fig. 6.3a for locations) indicate well-below-normal (and often record-setting) pressures during the austral winter, similar to Fig. 6.2c. Stations in East Antarctica and over the Ross Ice Shelf recorded much lower temperatures throughout the year. Climate data from two representative manned stations (Rothera and Halley) and two automatic stations (Dome C II and Gill) are displayed in Figs. 6.3b–e.

Monthly mean temperatures on the northern Antarctic Peninsula were near average at the start of the year but in winter and spring were significantly above average (not shown). Farther south on the Peninsula, Rothera recorded its warmest October temperature ever (-1.9°C; Fig. 6.3b). The monthly mean pressure at Rothera was above average at the start of the year with February recording its highest ever value of 994 hPa. After this, the monthly mean pressures were well-below average with June recording a new minimum of 979.4 hPa. Overall, this meant that Rothera recorded its lowest annual mean pressure of 984 hPa (Fig. 6.3b). Record-high wind speeds were also observed across many sites on the Peninsula in October; Ferraz station reported a record wind gust of 49.4 m s^{-1} on 15 October.

In the Weddell Sea region, the monthly mean temperatures at Halley were above average for all months except July when it was 0.2°C below average (Fig. 6.3c), resulting in the annual mean temperature at Halley being the third highest on record. Monthly mean temperatures at Neumayer Station started off higher than average but temperatures of about 5°C below average were recorded in June and July. Around the coast of East Antarctica, the monthly mean temperatures at Mawson, Davis, and Casey tended to oscillate between higher and lower than average, with very low

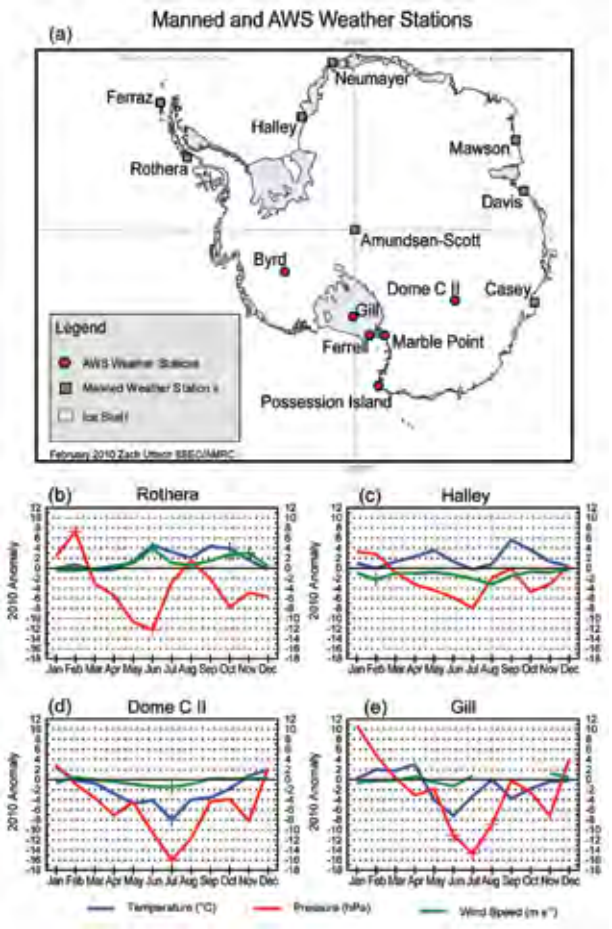

Fig. 6.3.(a) Locations of automatic and manned Antarctic weather stations described in Chapter 6. (b)–(e) 2010 Antarctic climate anomalies at four representative stations (two manned, two automatic). Monthly mean anomalies for temperature (°C), MSLP (hPa), and wind speed (m s^{-1}) are shown, with plus signs (+) denoting all-time record anomalies for a given month at each station. Climatological station data start in 1976 for Rothera, 1957 for Halley, 1980 for Dome C II, and 1985 for Gill. The base period for calculating the anomalies is 1979–2008 for manned stations, and the full record period for the automatic stations.

temperatures being recorded at Mawson and Davis in July and very high temperatures in September.

Monthly mean temperatures at Amundsen-Scott station at the South Pole varied over the year, sometimes significantly above average and sometimes below. In April, the temperature was 5.2°C below average at -62.6°C, which tied the lowest recorded April temperature back in 1998. In March, the values were 3.6°C above average, and 3.8°C above average in May.

Observations from automatic weather stations on the Polar Plateau, Ross Ice Shelf, and West Antarctica paint a very different picture for 2010 than was seen in 2009. Generally, above-average temperatures were found in the summer and fall, with below-average temperatures for the winter and spring. In addition, the stations reported lower pressures in the winter, with some low pressures breaking long-term records. On the Polar Plateau, Dome C II (Fig. 6.3d) had a record-low monthly mean temperature (8°C below the mean), a record-low monthly mean pressure, (16 hPa below the mean), and a record-low monthly mean wind speed (1.5 m s^{-1} below the mean) for July. In addition, the minimum temperature during the winter was below -73.3°C for April through September at Dome C II.

On the Ross Ice Shelf, Ferrell reported record-low pressures for July, August, and November (15 hPa, 9 hPa, and 7 hPa below the monthly mean, respectively), and Gill reported record-low pressures for June, July, and August (11 hPa, 15 hPa, and 9 hPa below the monthly mean, respectively; Fig. 6.3e). Closer to the Ross Sea, Marble Point also had a record-low pressure for July (14 hPa below the mean). In West Antarctica, record-low pressures for Byrd were below normal by 12 hPa for June and 17 hPa for July. Finally, at Possession Island near Cape Adare, record-low temperatures were 3°C below normal for both June and September and record low pressure was 11 hPa below the mean in July.

d. Net Precipitation—D. H. Bromwich and S.-H. Wang

Precipitation minus evaporation (P-E) closely approximates the surface mass balance over Antarctica, except for the steep coastal slopes (e.g., Bromwich et al. 2000; van den Broeke et al. 2006). Precipitation variability dominates P-E changes over the Antarctic continent. Precipitation and evaporation/sublimation fields from the Japanese Reanalysis (JRA; Onogi et al. 2007) were examined to assess Antarctic net precipitation behavior for 2010. The "evaporation" in JRA was calculated from the surface latent heat flux variable. In comparison to other long-term global reanalyses (e.g., NCEP1 and NCEP2), JRA has higher model resolution, both horizontally and vertically, greater observational usage, and a more advanced model configuration (Onogi et al. 2007). Nicolas and Bromwich (2011) show that the reliability of JRA P-E is highly ranked in relation to other contemporary global reanalyses.

Figure 6.4 shows the JRA annual anomalies of P-E and mean sea level pressure (MSLP) for 2010 (Figs. 6.4a,c) and 2009 (Figs. 6.4b,d). In general, the annual anomalies over the high interior of the continent are small (within ± 50 mm yr^{-1}), consistent with the low amount of snow accumulation in this region. Most

coastal regions in 2010 display more negative P-E anomalies than during the previous year, with the exception of the Weddell Sea and Ellsworth Land (90°W). The most negative P-E anomalies can be observed to the west of the Antarctic Peninsula in 2009 (between 60°W and 150°W, centered in the Amundsen Sea, Fig. 6.4b), in contrast to both positive and negative anomalies in the same region in 2010 (Fig. 6.4a). Less precipitation (P-E) can also be found over Ross Sea and the northern edge of Queen Maud Land (between 0° and 60°E) during 2010 than during 2009. These annual P-E anomaly features are consistent with the mean atmospheric circulation implied by the MSLP anomalies (Figs. 6.4c,d). In 2009, a negative anomaly centered over the Drake Passage was observed; in 2010, a much deeper negative anomaly was observed in the Amundsen-Bellingshausen Seas (~105° W), mainly due to the negative anomalies in May–November (Figs. 6.2c,e). The latter produced stronger offshore flow and less precipitation along the coast from Pine Island Bay to the Ross Ice Shelf, and in combination with positive MSLP anomalies over the South Atlantic (Fig. 6.4c), brought more moisture to the Antarctic Peninsula and Weddell Sea region. Secondary negative MSLP anomalies observed along the East Antarctic coast in 2010 at 75°E and 120°E produced positive P-E anomaly features near Davis (80°E) and Dumont d'Urville (135°E) stations, respectively.

The austral fall (March–May) P-E anomalies (not shown) had the largest impact on 2010 annual anomalies, especially west of the Antarctic Peninsula, where they contributed more than 50% of the total annual P-E anomalies. The influence of La Niña on P-E is also noted, as the persistent low pressure in the Amundsen-Bellingshausen Seas since April (Figs. 6.2c,e,f) indicates greater-than-normal storm activity during most months of 2010, ultimately resulting in the large P-E anomaly just west of the Antarctic Peninsula (positive) and for Marie Byrd Land-Ross Ice Shelf (negative). Earlier studies suggest that such anomaly features are consistent with simultaneous strong La Niña (Bromwich et al. 2000, 2004) and positive SAM events (Fogt and Bromwich 2006; Fogt et al. 2011). Figure 6.4e shows the time series of average monthly total P-E over Marie Byrd Land (75°S–90°S, 120°W–180°) and monthly SOI and SAM indices (with 12-month running means). It is clear that SOI and SAM are in phase with each other but

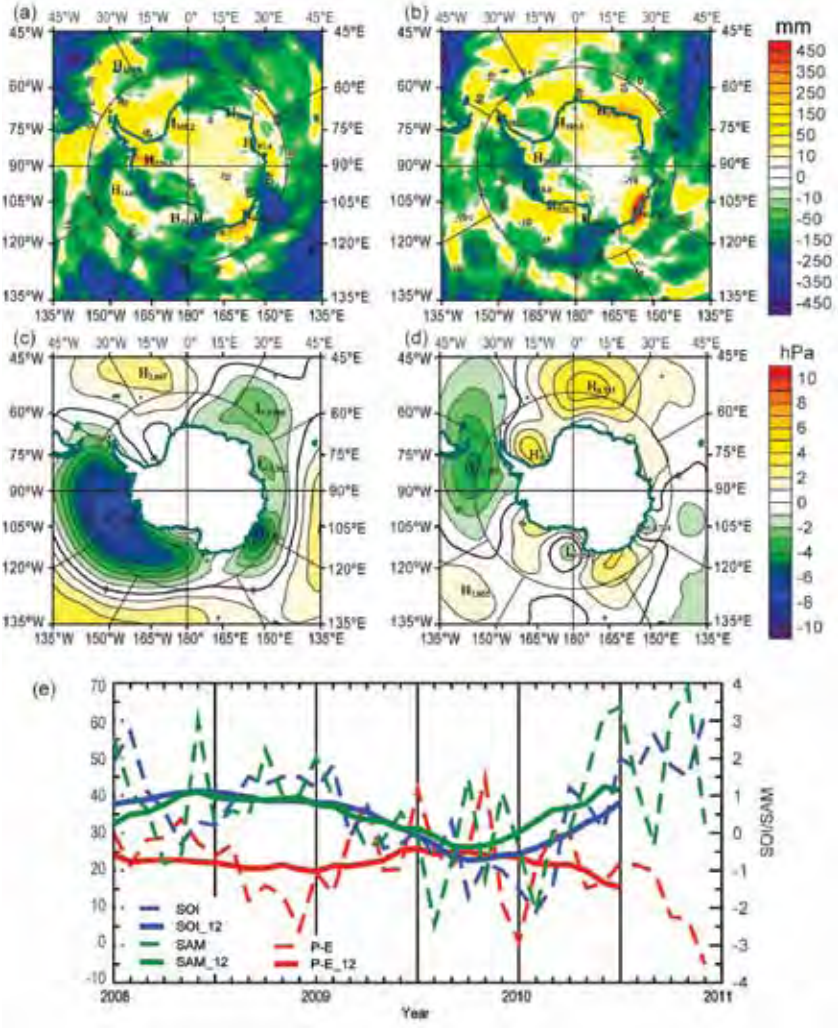

Fig. 6.4. (a–d) Annual precipitation minus evaporation (P-E) and annual mean sea level pressure (MSLP) anomalies: (a) 2010 P-E anomalies, departure from the 1979–2009 mean; (b) 2009 P-E anomalies, departure from the 1979–2008 mean; (c) 2010 annual MSLP anomalies; and (d) 2009 annual MSLP anomalies. (e) Monthly total P-E (mm; red) for the West Antarctic sector bounded by 75°S–90°S, 120°W–180°, along with the SOI (blue, from Climate Prediction Center) and SAM [green, from Marshall (2003)] indices since 2008. Centered annual running means are plotted as solid lines. (P-E data are from JRA-25 reanalysis.)

SIDEBAR 6.1: PINE ISLAND GLACIER, WEST ANTARCTICA—E. RIGNOT

Pine Island Glacier (75°S, 100°W; Fig. 6.5), in West Antarctica is a gigantic ice stream that discharges about 100 trillion tons of ice into the Amundsen Sea every year, one of the largest amounts in Antarctica (Rignot et al. 2008). This glacier was identified as a potential weak spot in Antarctica back in the 1970s because it is grounded well below sea level and is not buttressed by a large floating extension at sea (Hughes 1981). In the late 1990s, satellite data revealed for the first time this glacier was undergoing major changes; its line of grounding was retreating at a rate of 1 km yr^{-1} (Rignot 1998). Since then, additional data have shown that the glacier is accelerating and thinning (Wingham et al. 2009). During the last 18 years, the rate of glacier thinning has quadrupled, and its ice velocity has increased by more than 66%, rising more every year than the previous year (Rignot 2008). In late 2009, for the first time since 1992, the glacier speed stabilized and stopped its exponential increase (Joughin et al. 2010). The grounding line has now retreated by more than 20 km since 1992. The glacier has become afloat over a large sector that previously was only a few tens of meters above flotation. It is also now retreating into much deeper ice (getting deeper inland), a configuration that has been hypothesized to be unstable by glaciologists in the 1970s.

Recent data collected in situ by autosubmarine (Jenkins et al. 2010) and on airplanes using airborne gravity (Studinger et al. 2010) unveiled the presence of a major ridge beneath the floating ice shelf in front of the glacier that probably anchored the glacier back in the 1960s–1970s. Since 1996, this glacier has been coming in contact with warm waters by Antarctic standards, which regularly ablate large amounts of glacier ice from below every year (Jacobs et al. 1996). It is uncertain how much of the current retreat is driven by the detachment of the glacier from its former pinning point decades ago, and/or how much is caused by the advection of warmer water from the circumpolar current underneath the glacier in recent years.

However, the glacier is already a major participant in the overall mass budget of the Antarctic Ice Sheet—which is losing mass to the sea and raising sea level—and that it, along with its neighbors, if completely melted constitutes enough ice to raise global sea level by more than one meter. The glacier and its surrounding areas are now receiving international attention and are routinely monitored by satellites and surveyed by airborne platforms since the first field party in the 1980s. These data will bring new insights into the current and future evolutions of this region and, in particular, reexamine if models predicting that the glacier will soon resume its acceleration and triple its ice velocity are realistic or not (Thomas et al. 2004).

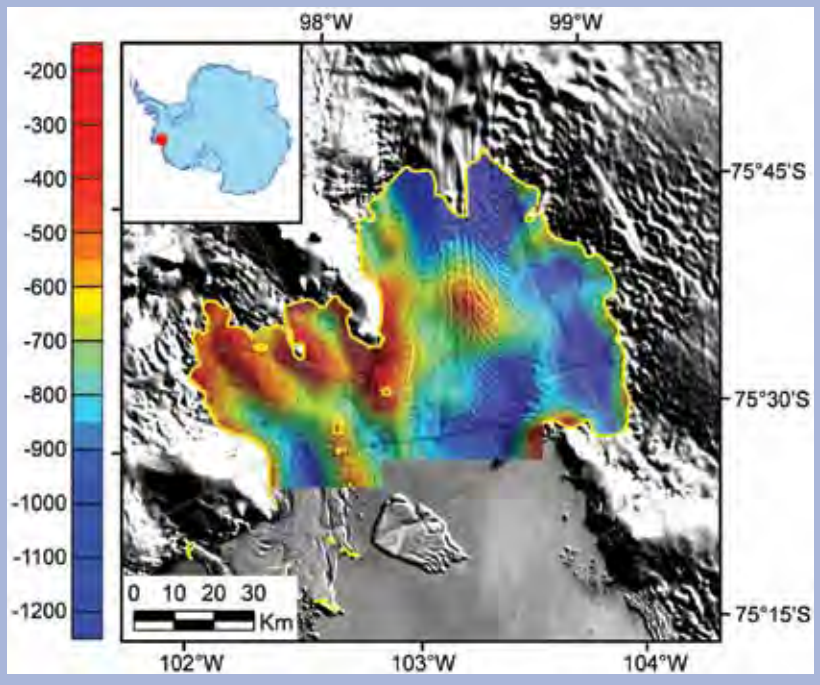

Fig. 6.5. Sea floor topography beneath the floating ice shelf in front of Pine Island Glacier, West Antarctica unveiled by the NASA-Icebridge mission in November 2009 using airborne gravity and showing a previously unknown sub-ice-shelf ridge at 76°S, 104°W that may have anchored the glacier five to six decades ago. Bed elevation color coded from blue (deep) to red (high) overlaid on a MODIS mosaic of Antarctica (Courtesy M. Studinger, NASA GSFC, 2010).

have opposite behavior to P-E in most months from 2008 onward. The correlation coefficients between monthly P-E and index values are highly significant: SOI -0.31 (-0.48 for annual running mean) and SAM -0.32 (-0.77 for annual running mean), respectively.

e. *2009/10 Seasonal Melt Extent and Duration*—L. Wang and H. Liu

Surface snow melt on the Antarctic ice sheet during the 2009/10 austral summer was estimated from the space-borne Special Sensor Microwave Imager (SSM/I) passive microwave observations at the 19 GHz horizontal-polarization channel. A wavelet-transform based edge detection method (Liu et al. 2005) is applied to track melt onset and end dates from time series of daily brightness temperatures for individual SSM/I pixels. The total annual melt duration is calculated by accumulating the number of melt days between each pair of onset and end edges. Figures 6.6a–c display the melt start day, melt end day, and melt duration, respectively.

Melt mainly occurred along the Antarctic coastline in austral summer 2009/10. The total area that experienced surface melt was 945 000 km^2, which is considerably larger than last year (681 900 km^2; L. Wang et al. 2010). However, this value is still below the 30-year average (1 290 700 km^2), below the 25-year median melt extent (1 277 500 km^2) reported in Liu et al. (2006), and below the 20-year average (1 280 000 km^2) reported in Torinesi et al. (2003). This year's melt index (calculated by accumulating the number of melting days over the entire Antarctic ice sheet; Liu et al. 2006) is 39 349 375 day km^2, which is almost double the amount of last year (20 533 000 day km^2; L. Wang et al. 2010). A larger melt index implies either an extended melt area or a longer melt season. The melt peak day was 9 January, with three other smaller peaks on 1 February, 13 February, and 6 March (Fig. 6.6d). The major melt season is from mid-December 2009 to mid-January 2010. Some short-period melt happened in late March. The off-season melt was mainly distributed on Wilkins Ice Shelf (Fig. 6.6b).

Most melt areas are located at latitudes equatorward of 75°S, including the ice shelves along the Antarctic Peninsula, Wilkins, Queen Maud Land, Amery, Shackleton, and Abbot (see Fig. 6.6 for locations). High-latitude melt is mainly found on Marie Byrd Land. There is still no surface melt or very small amount of melt detected on the Ronne-Filchner Ice Shelf, Ross Ice Shelf, Victoria Land, and Wilkes Land. Compared to the 2008/09 austral summer, extensive surface melt occurred on the coast of Queen Maud Land. The melt index for this sub-region is 11 908 125 day km^2. Comparing to the 25-year average melt index (7 471 500 day km^2; Liu et al. 2006) in Queen Maud Land, this year can be considered as an exceptionally high melting year for this area.

f. Sea Ice Extent and Concentration—R. A. Massom, P. Reid, S. Stammerjohn, S. Barreira, and T. Scambos

During 2010, zonally-averaged Antarctic sea ice extent was characterized by fluctuations that were closely associated with changes in large-scale atmospheric circulation patterns. Sea ice extent from January through late April was generally near to below average compared to the 1979–2008 mean (Fig. 6.7a), although major regional contrasts are apparent during this time. This pattern, and the underlying climate pattern in the far south, changed significantly for the period June–December. In general, a strong positive sea ice extent anomaly was observed during this time.

During the January–May period, there were strong positive anomalies in ice concentration and extent in the Weddell Sea, western Ross Sea, and western Pacific Ocean, balanced by strong negative anomalies in the Amundsen-Bellingshausen, outer Ross Sea, and Indian Ocean sectors (Fig. 6.7b). These patterns are indicative of large-scale wind patterns associated with atmospheric pressure fields (i.e., Fig. 6.2a) and are largely consistent with the regional 30-year trends in seasonality and extent (Comiso 2010; Stammerjohn et al. 2008). Early in the year, the negative anomaly in the Bellingshausen Sea coincided with a 30-year maximum in SST in that sector (Lee et al. 2010). An additional factor observed in the northwest Weddell Sea in the 2009/10 summer was the presence of ice blocks derived from the rapid retreat/disintegration of glaciers in the region, which impacted shipping operations by increasing local sea ice cover.

In May, the zonally-averaged sea ice extent anomaly changed to strongly positive, i.e., up to 2 standard deviations above the 1979–2008 mean (Fig. 6.7a). This major change coincided with Southern Hemisphere circulation anomalies that were consistent with transitions from a negative to positive polarity of the SAM index and El Niño to La Niña conditions in the tropical Pacific (i.e., section 6b; Fig. 6.2). Furthermore, Fig. 6.7a indicates that the zonally-averaged sea ice extent anomaly from mid-June through late August was the largest in the 30+ year record. Changes in two regions in particular were responsible for the major increase in overall ice extent at this time (May–June), namely: (1) a switch from negative to strongly positive ice-edge anomaly across eastern Ross to Amundsen

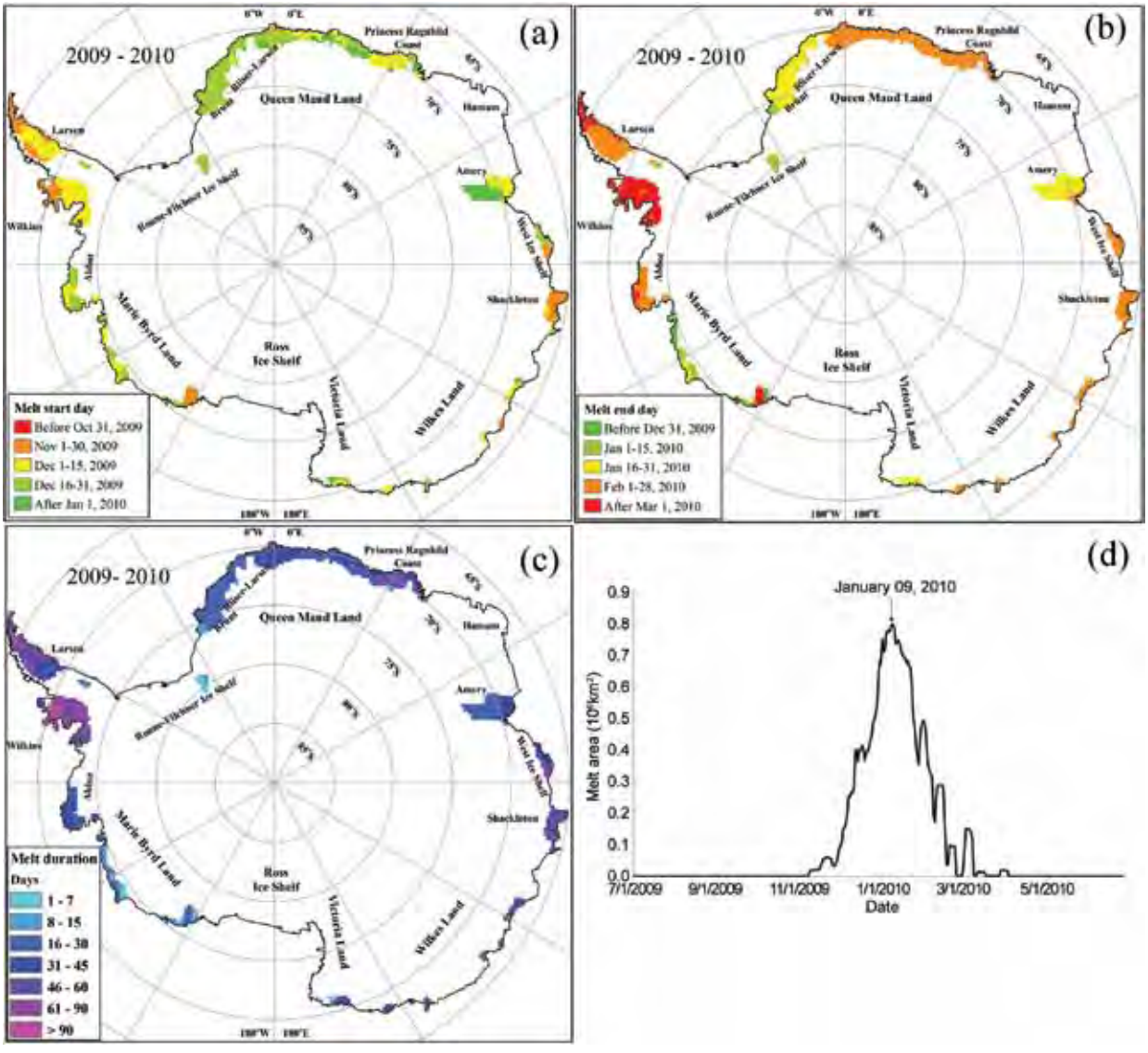

Fig. 6.6. Maps for (a) melt start day, (b) melt end day, and (c) melt duration of the Antarctic ice sheet during 2009/10 austral summer. Daily melt extent is shown in (d) with melt peak day indicated.

Seas sector and (2) the development of an extensive positive anomaly of similar magnitude off Enderby Land (Indian Ocean sector). These positive ice-edge anomalies are likely to be due to a combination of over extensive fronts, wind-driven ice advection and in situ thermodynamic growth, the latter associated with the development of cold pools of SST (particularly in the eastern Ross Sea from about June onwards). Elsewhere, sea ice extent was average to below average in May–June. The circumpolar pattern of extensive zones of strongly positive and more moderate negative ice-edge anomalies shown in Fig. 6.7c generally persisted from June through late December 2010 (with the positive regional ice-extent and concentration anomalies intensifying in late November through early December).

The pattern of regional sea ice anomalies in the Western Hemisphere described above and for the period from May–June onwards is consistent with the presence of a persistent negative mean sea level pressure (MSLP) anomaly in the Amundsen Sea region in May–November (Figs. 6.2c,e) and along the Antarctic Peninsula in December (Fig. 6.2g). Studies have demonstrated that negative MSLP anomalies in this region are commonly observed and displaced east of their mean location during La Niña events and during the positive polarity of the SAM index (Fogt and Bromwich 2006; Stammerjohn et al. 2008), although other local factors can also play a role. In general,

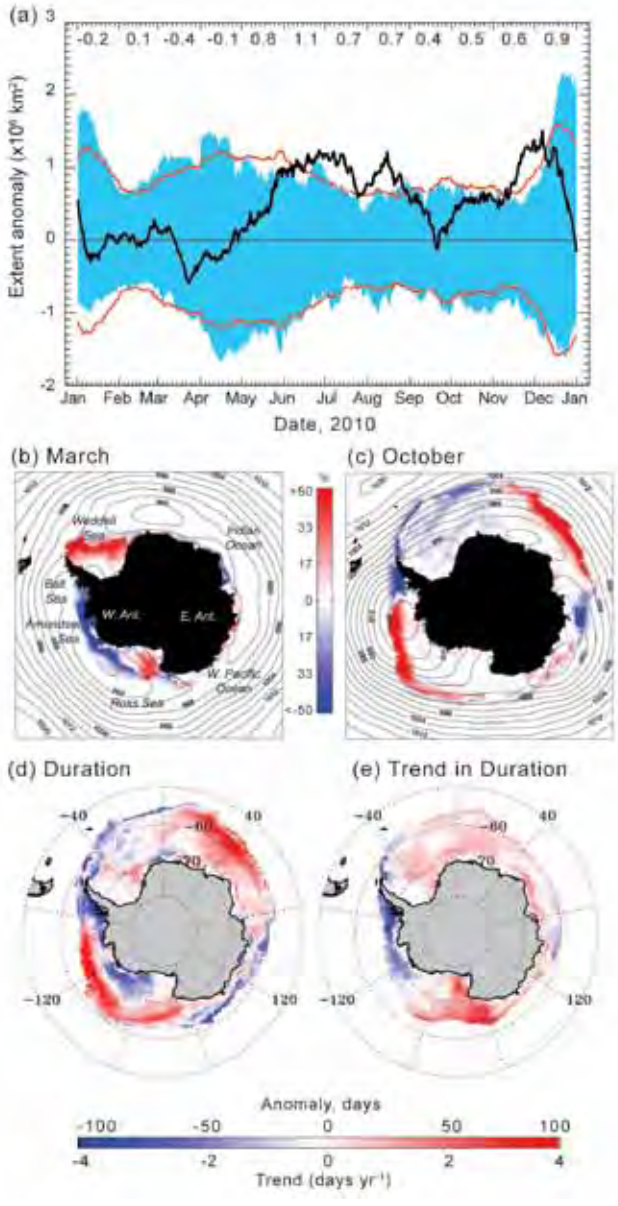

Fig. 6.7. (a) Plot of daily anomaly (black line) from the climatology (1979–2008) of daily Southern Hemisphere sea ice extent for 2010, based on satellite passive microwave ice concentration data from the GSFC Bootstrap Version 2 dataset (Comiso 1999, updated 2008). Blue banding represents the range of daily values for 1979–2008, while the red line represents ±2 standard deviations. At the top are monthly-mean extent anomalies (x10^6 km^2). (b–c) Sea ice concentration anomaly maps for March and October 2010 derived versus the monthly means for 1979–2007, with monthly-mean contours of MSLP [from the Australian Community Climate and Earth System Simulator (ACCESS)] provided by the Australian Bureau of Meteorology. (d) Sea ice duration anomaly for 2010/11, and (e) duration trend. For (d) and (e), see Stammerjohn et al. (2008) for a description of techniques (using daily satellite passive-microwave data). Both the climatology (for computing the anomaly) and trend are based on 1979/80–2007/08 data, for which GSFC Bootstrap Version 2.0 data were available (Comiso 1999, updated 2008), while the 2010/11 duration-year data are from the NASA Team Near-Real-Time Sea Ice (NRTSI) dataset (Maslanik and Stroeve, 1999). The 2010/11 duration anomaly is therefore the 2010/11 NRTSI data minus the 1979/80–2007/08 BS V2 Climatology. Discrepancies introduced by using these different data sources lead to an uncertainty (difference) level that is well below the magnitude of the large changes/anomalies.

the large zonally-averaged sea ice extent anomaly from June through December (with the exception of September; Fig. 6.7a) is consistent with the presence of negative temperature anomalies in the Pacific Ocean and the concurrent circumpolar pattern of increased westerly winds associated with a strong positive SAM index (Fig. 6.1c); the latter helps to drive the ice edge equatorward (via Ekman drift). Embedded within that zonally-forced atmospheric pattern are the more regional-scale anomalies (described above) associated with a predominantly wave-2 pattern for most of the latter half of the year.

An abrupt dip in zonally-averaged extent for a brief period in mid-September (Fig. 6.7a) was the result of increased cyclonic activity centered on 90°E which saw sea ice extent off the east coast of Antarctica (in the approximate sector 70°E–120°E) fall dramatically. At the same time, a major negative extent/concentration anomaly developed in the Bellingshausen Sea/West Antarctic Peninsula sector. Below-average sea ice extent and concentration persisted throughout the year in this sector, apart from a brief wintertime rebound to above-average in July–August. This pattern is again consistent with long-term trends in this region (Comiso 2010; Stammerjohn et al. 2008).

In terms of seasonality, the spatio-temporal pattern of Southern Hemisphere sea ice duration in 2010 was affected by a very late sea ice advance across the Bellingshausen-Amundsen Seas sector (not shown). Again, this appears to be consistent with the atmospheric circulation anomalies in May–July described above, and especially the low-pressure anomaly around 150°W–160°W (Fig. 6.2c). The annual retreat pattern (not shown) resembles the classic high-latitude response to La Niña (section 6b), with the low pressure anomaly moving towards, and in November–December straddling, the Antarctic Peninsula (Figs. 6.2c,e,g). East Antarctica has two distinct patterns in terms of duration anomaly, namely predominantly longer in the Indian Ocean

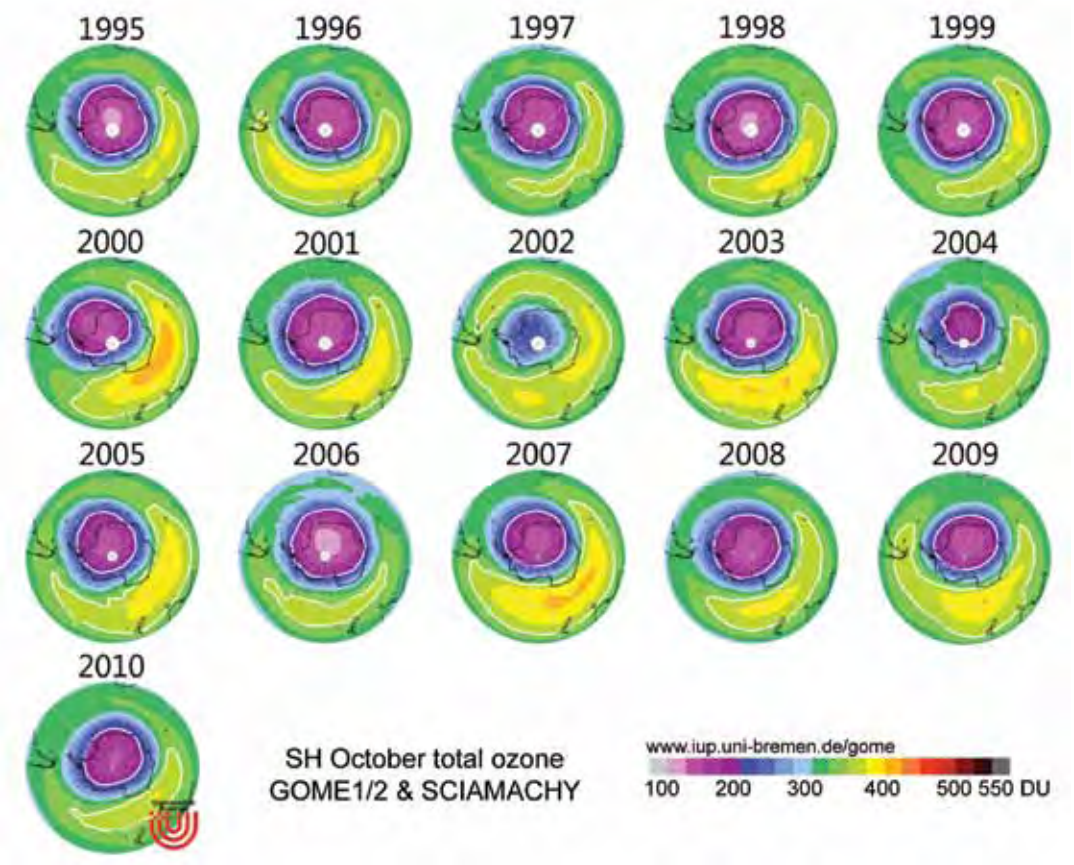

Fig. 6.8. October averages of total column ozone derived from the GOME 1 and 2, and SCIAMACHY instruments (courtesy of Prof. John Burrows, Univ. of Bremen).

(consistent with the long-term trend in Fig. 6.7e) but shorter over much of the West Pacific sector (where the long-term trend is generally positive).

g. Ozone Depletion—P. A. Newman, E. R. Nash, C. S. Long, M. C. Pitts, B. Johnson, M. L. Santee, and J. Burrows

The 2010 Antarctic ozone hole was in the low range of severity. Prior to 1980, severe ozone losses over Antarctica were not apparent. After 1990, every year has seen a severe loss. Compared to the 1990–2009 period, the 2010 ozone hole average area and the average minimum total ozone was in the lowest 20% of observed values. Figure 6.8 displays October averages of total ozone derived from the GOME/SCIAMACHY instruments from 1995 to 2010. Using Ozone Monitoring Instrument (OMI) total ozone observations, the area of the 2010 hole was approximately 19.0 million km^2, averaged over the period of most severe depletion from 7 September to 13 October. The peak area was observed on 25 September at 22.2 million km^2. This value is comparable to the smaller ozone hole of 2004 but larger than the record low area of 2002. The average depth of the ozone hole was 127 Dobson Units (DU), averaged over the period of lowest ozone from 21 September to 16 October (the lowest observed value was 118 DU on 1 October). In addition to the small area, the ozone hole began developing in mid-August rather than the early August period. Slightly different values for the area and depth of the ozone hole are found by the SCIAMACHY and NOAA SBUV/2 instruments, but the patterns are consistent between all of the satellite instruments.

Vertical profiles of ozone from the NOAA South Pole station (not shown) indicate that ozone dropped to a zero value by late September at altitudes of 16 km–17 km. These NOAA balloon-borne ozone instruments revealed that ozone values were near zero between 14 km and 20 km by 6 October 2010, and that these very low values persisted to mid-October. This vertical profile information forms a consistent picture with the observations from the total ozone instrumentation.

The ozone hole is caused by the conversion of chlorine molecules from the non-reactive forms into ozone reactive forms on the surfaces of polar stratospheric clouds or PSCs (i.e., $HC1+C1ONO_2 \xrightarrow{PSC}$

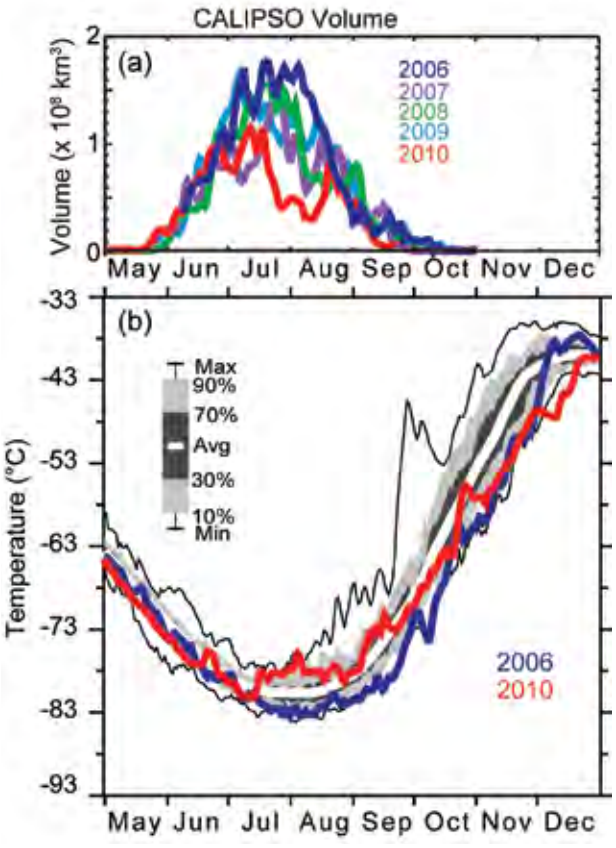

Fig. 6.9. (a) Daily time series of CALIPSO PSC volume for the Antarctic winter season (updated from Pitts et al. 2009). (b) Climatology of daily temperature averages for 50 hPa, 60°S–90°S as derived from 1979–2010 data. The red line shows 2010, while the blue line shows 2006. The thick white line shows the average for each day of this climatology. The gray shading shows the percentage range of those same values. The data are from NCEP CPC stratospheric analyses.

Cl_2 + HNO_3). The molecular chlorine photolyzes as the sun rises in spring, and this chlorine (combined with bromine) directly causes catalytic ozone loss. CALIPSO satellite observations show that in late September 2010, PSC volume was the lowest observed over their 2006–10 Antarctic observations record (Fig. 6.9a), and was virtually zero by late September (update from Pitts et al. 2009). Ozone-depleting substances (ODSs) in the 2010 Antarctic ozone hole are estimated to have only decreased by about 5.3% (3.8 ppb) from the peak levels in the 2000–02 period (4.0 ppb). These ODSs have fallen 11% towards the 1980 level of 2.1 ppb.

The Microwave Limb Sounder (MLS) on the NASA Aura satellite measures the abundances of both nonreactive (HCl) and ozone-destroying (ClO) forms of chlorine and is thus able to track the activation and deactivation of chlorine as it is interconverted between them. Consistent with the unusually small volume of air exposed to PSCs (Fig. 6.9a), the enhancement of ClO (i.e., the magnitude of chlorine activation) was considerably weaker in 2010 than in other recent Antarctic winters. Not only were ClO abundances smaller, but also the enhancement did not extend as high in altitude as typical.

The temperature variability of the Antarctic stratosphere modulates the severity of the ozone hole from year to year. Lower-than-average Antarctic temperatures result in larger and deeper ozone holes, while higher temperatures lead to weaker ozone holes (Newman et al. 2004). Figure 6.9b shows the temperature time series (from NCEP) for 50 hPa averaged from 60°S–90°S. The 2010 July–September period was near or above average (see also Fig. 6.1b). The sharp increases of temperature in both mid-July and early September are accompanied by sharp decreases of PSC volume (Fig. 6.9a). Hence, the comparatively smaller 2010 ozone hole is primarily a result of the higher-than-average temperatures. This warming is a result of large wave events in mid-July and early September that sharply increased the temperature (Figs. 6.9 and 6.1b).

The 2010 ozone hole was unusually persistent. Low ozone values (< 220 DU) continued into mid-December 2010. Very weak wave forcing occurred during the late October to early December period. The depleted region of ozone remained centered on Antarctica until a large wave event in mid-December finally caused the ozone hole to disappear.